Filamentation processes and dynamical excitation of light condensates in optical media with competing nonlinearities

David Novoa, Humberto Michinel, Daniele Tommasini, and Alicia V. Carpentier

Departamento de Física Aplicada, Facultade de Ciencias de Ourense, Universidade de Vigo, As Lagoas s/n, ES-32004 Ourense, Spain

We analyze both theoretically and by means of numerical simulations the phenomena of filamentation and dynamical formation of self-guided nonlinear waves in media featuring competing cubic and quintic nonlinearities. We provide a theoretical description of recent experiments in terms of a linear stability analysis supported with simulations, showing the possibility of the observation of modulational instability suppression of intense light pulses traveling across such nonlinear media. We also show a mechanism of indirect excitation of light condensates by means of coalescence processes of nonlinear coherent structures produced by managed filamentation of high-power laser beams.

I. INTRODUCTION

Studies of nonlinear beam filamentation of ultrashort pulses are being actively developed nowadays [1]. Far beyond a certain critical power threshold, extremely short pulses may become unstable and break up into several uncorrelated light structures by modulational instability (MI) processes. These structures, called *filaments* in this context, are spatiotemporal soliton-like light distributions which appear after MI and hold for large propagation distances without changing their shape or size [2]. In fact, optical filaments have been observed in several scenarios, such as air [1], water [3], and carbon disulfide [4], and some mechanisms to control their spatial location have been recently proposed [5].

On the other hand, the theoretical description of these localized modes is generally based on nonlinear Schrödinger equations (NLSEs) [6–8]. In the modeling of these kind of systems, nonlinear effects like two- and three-photon absorption, second-order group-velocity dispersion, time-delayed nonlinear response, multiphoton ionization, and plasma defocusing [9] are usually taken into account. Nevertheless, in order to favor the insight of dynamics in these systems, simpler models are employed when certain physical conditions are satisfied. To this end it is common to consider NLSEs involving only local intensity-dependent nonlinear susceptibilities which are real [9]. As an example, the so-called cubic-quintic (CQ) nonlinearity [10] has been used as a solvent approximation in modeling subpicosecond pulse propagation in nonlinear media [4]. In Ref. [4], the dynamics of filament formation and evolution in carbon disulfide cells is analyzed both experimentally and by numerical means. In this respect, extensive numerical work based on a conservative CQ model is successfully employed in the qualitative description of experimental achievements.

In addition, "liquid light condensates" (i.e., robust solitonic distributions in CQ optical media with a "flat-top" transverse spatial envelope and intriguing surface tension properties) were studied in Ref. [11]. Recently, it was shown that their dynamics follows the same equations governing the evolution of usual liquid droplets [12]. These results were obtained by both analytical and numerical methods, but they have not yet been confirmed by real experiments. The main difficulty, of course, is the search for a cubic-quintic nonlinear medium,

although some candidates were inspected in Ref. [13]. In fact, both nonlinear third- and fifth-order terms in the polarization of the material are usually complex, so it is often necessary to consider some other nonlinear processes like those mentioned above. Nevertheless, in light of Ref. [4], we are allowed to think of materials like CS_2 as real CQ nonlinear media in specific power regimes. Recently, some common gases such as air, N_2, and O_2 have also been identified as CQ optical media by means of the measurement of n_4 coefficients [14], although the propagation dynamics of probe pulses throughout these media has not yet been investigated.

The purpose of the present paper is threefold. First, we give a simple theoretical description of the results obtained in Ref. [4] by means of a linear stability analysis of plane waves. Second, we study both analytically and numerically the possibility of real observation of the modulational instability suppression process in CS_2. Finally, we provide a detailed description of a mechanism of dynamical excitation of flat-top solitons in "pure" CQ systems via filamentation management and coalescence and we analyze the possibility of achieving light condensates in carbon disulfide.

II. PHYSICAL MODEL

We consider the propagation of a high-intensity laser pulse through a CS_2 bulk, within the framework of the NLSE. In order to simplify the theoretical model, we assume a scalar slowly varying spatial envelope and we neglect group-velocity dispersion effects. These approximations have been experimentally justified for media like carbon disulfide [4] and air [9] within proper parameter spaces. We also include a cubic-quintic nonlinearity, resulting in the following NLSE:

$$2ik_0 n_0 \frac{\partial \psi}{\partial z} + \nabla_\perp^2 \psi + 2k_0^2 n_0 (n_2 |\psi|^2 - n_4 |\psi|^4)\psi = 0, \quad (1)$$

where ψ is the complex slowly varying electric field envelope of the corresponding electromagnetic wave propagating through the nonlinear medium, $k_0 = 2\pi/\lambda$ is the vacuum wavenumber corresponding to the laser source wavelength λ, n_0 is the linear refractive index of the medium, and z is the propagation distance. Nonlinear coefficients n_2, n_4 characterize the strength of the real third- and fifth-order nonlinear optical

susceptibilities, respectively, and $\nabla_\perp^2 = \partial^2/\partial x^2 + \partial^2/\partial y^2$ is the Cartesian transverse Laplacian operator. Notice that Eq. (1) preserves the norm of the field Ψ; that is, we have also neglected the effect of nonlinear two-photon absorption, which can be justified for moderate-intensity pulses traveling throughout a carbon disulfide bulk over a short distance [4].

For technical reasons related to numerical treatment of partial differential equations, it is often useful to express Eq. (1) in a reduced form by introducing a suitable set of nondimensional variables, namely

$$i\frac{\partial \Phi}{\partial \eta} + \Delta \Phi + (|\Phi|^2 - |\Phi|^4)\Phi = 0, \qquad (2)$$

where $\eta = zk_0 n_2^2/n_4$ is the nondimensional propagation distance, $\Delta = \partial^2/\partial \chi^2 + \partial^2/\partial \zeta^2$ is the dimensionless transverse Laplacian operator, with spatial coordinates $\Theta = \theta k_0 n_2 \sqrt{2n_0/n_4}$, with $\Theta = \chi, \zeta$, $\theta = x, y$. The normalized beam irradiance $|\Phi|^2 = (n_4/n_2)|\psi|^2$ is measured in units of the quotient n_4/n_2 which univocally characterizes the nonlinear response of the medium.

Keeping in mind the equivalence between Eqs. (1) and (2), typical parameters corresponding to beam propagation in real dielectric materials like CS_2 are (for femtosecond optical pulses with $\lambda = 800$ nm [15]) $n_0 = 1.6$, $n_2 = 3 \times 10^{-15}$ cm^2/W. To our best knowledge, the CS_2 quintic coefficient n_4 has not yet been measured, since there are no values of this quantity cited in the literature, although an approximation of $n_4 = 2 \times 10^{-27}$ cm^4/W^2 based on the agreement between simulations and experiments was successfully introduced in Ref. [4]. Very remarkably, the first experimental determination of the nonlinear coefficient n_4 of several gaseous media was recently carried out in Ref. [14].

In the following section, we introduce an analytical linear stability analysis of plane waves in the CQ model and its results are compared with those of the experiments in Ref. [4].

III. LINEAR STABILITY ANALYSIS OF PLANE WAVES

It is well known that Eq. (2) admits plane-wave (PW) solutions of the type $\Phi = \Phi_0 e^{i\gamma\eta}$, where Φ_0 is a constant which depends on γ eigenvalues as follows:

$$\Phi_0 = \left(\frac{1}{2} + \frac{\sqrt{1-4\gamma}}{2}\right)^{\frac{1}{2}}. \qquad (3)$$

Let us proceed with a linear stability analysis of these homogeneous solutions, following the Bespalov-Talanov procedure [16]. The first step of this method is to add a small amplitude perturbation of the form $\xi = \xi_R + i\xi_I$ to the PW solutions, with $\xi_{R,I} = \xi_{R,I}^0 e^{[i\mathbf{K}_\perp \cdot \mathbf{r} + ih\eta]}$ and $|\xi_{R,I}| \ll \Phi_0$, where $\mathbf{K}_\perp$ is the transverse wave vector and h is the propagation constant of the corresponding perturbational mode. Now, for $h^2 < 0$, depending on the sign of $\text{Im}(h)$, we have two possible outcomes. If $\text{Im}(h) < 0$, the perturbations grow exponentially in η, yielding to field destabilization. However, if $\text{Im}(h) > 0$, the amplitude of the perturbational mode decays quickly, so that the underlying PW remains stable. On the contrary, whenever $h^2 > 0$, the amplitude of the perturbations remains limited.

By substituting the expression for the perturbed PW $\Phi = (\Phi_0 + \xi)e^{i\gamma\eta}$ in Eq. (2) and separating both the real and imaginary parts of the outgoing relation, we obtain, after linearizing on ξ_R, ξ_I (i.e., retaining only the first-order terms in perturbation theory), the following pair of Schrödinger-type equations:

$$\frac{\partial \xi_I}{\partial \eta} - \Delta \xi_R - \left(2\Phi_0^2 - 4\Phi_0^4\right)\xi_R = 0, \qquad (4a)$$

$$\frac{\partial \xi_R}{\partial \eta} + \Delta \xi_I = 0, \qquad (4b)$$

where $\xi_{R,I}$ depend upon $K_\perp$ and h in the way noted above. From Eq. (4b), we obtain $\xi_R = \frac{K_\perp^2}{ih}\xi_I$, and taking into account Eq. (4a) we deduce the algebraic relation

$$\Gamma = K_\perp\left(-K_\perp^2 + 2\Phi_0^2 - 4\Phi_0^4\right)^{\frac{1}{2}}, \qquad (5)$$

where Γ is the growth rate of the perturbations, satisfying $\Gamma = ih$. Notice that all the information about the PW perturbational spectrum is contained in the amplitude Φ_0. We can estimate the value of the transverse wave vector which gives the maximum growth rate by looking for the extremals of Eq. (5); that is,

$$\frac{\partial \Gamma}{\partial K_\perp} = 0 \to (K_\perp^{\max})^2 = \Phi_0^2 - 2\Phi_0^4 = \Gamma_{\max}. \qquad (6)$$

As a consequence, the PW of amplitude $\Phi_0 = \frac{1}{2}$ features the highest perturbation growth rate (see Fig. 1). This means that it will suffer destabilization in a shorter characteristic scale than any other homogeneous solutions of Eq. (2) if it is perturbed by a harmonic mode with $K_\perp = K_\perp^{\max}$. These assertions are illustrated by Figs. 1 and 2. In Fig. 1 the quantity $\Gamma_{\max}$ is plotted as a function of the PW intensity. For $|\Phi_0|^2 > 0$, we get $\Gamma_{\max} \leqslant 0$, corresponding to the modulationally stable PW branch [17]. The three pseudocolor intensity plots in the right-hand side of Fig. 1 display different examples of the state of perturbed
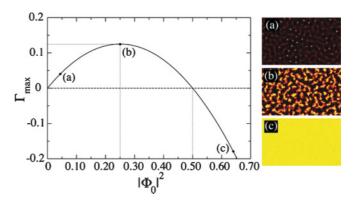

FIG. 1. (Color online) Plot of $\Gamma_{\max}$ vs $|\Phi_0|^2$. The highest growth rate corresponds to $\Phi_0^2 = 0.25$, whereas for $\Phi_0^2 \geqslant 0.5$ all values of $\Gamma_{\max}$ vanish or become negative, delimiting the domain of modulational instability suppression. The labeled points on the graph refer to the pseudocolor intensity plots to the right of the graph. These plots display a small region (width $= 500$, height $= 300$) of perturbed PWs of intensities (a) $\Phi_0^2 = 0.045$, (b) $\Phi_0^2 = 0.25$, and (c) $\Phi_0^2 = 0.64$ at the propagation distance $\eta = 125$. The filaments shown in (b) arise before those in (a), so that both coalescence and domain formation effects can be observed.
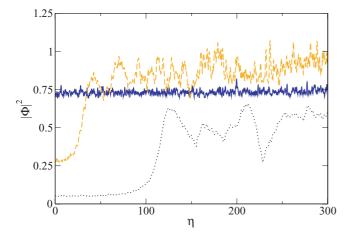
FIG. 2. (Color online) Plots of the peak intensity evolution over the line $[\zeta = 0, -120 < \chi < 120]$ of perturbed plane waves. The solid (blue) line ($\Phi_0^2 = 0.64$) is almost constant, featuring small bounded oscillations due to spatial noise initially added. The dashed (orange) line ($\Phi_0^2 = 0.25$) shows a rapid growth in intensity with η, which is a trace of a short longitudinal instability scale. The dotted (black) line ($\Phi_0^2 = 0.045$) shows the destabilization scale for experimental data [4]. It is important to notice the difference in between the instability scales of the dashed (orange) and dotted (black) curves. For the simulation with experimental data, the starting point of the filamentation process is around $\eta = 75$ (2.1 mm in dimensional units), which is compatible with that of experiments. In all cases, the maximum propagation distance is $\eta = 300$.

light homogeneous distributions after a propagation distance $\eta = 125$. All PWs considered throughout this manuscript are perturbed with a 5% spatial random noise and propagated with a standard beam propagation method.

Figure 1(a) corresponds to a simulation with $\Phi_0^2 = 0.045$ (unstable PW). It is observed that this noisy distribution leads to the formation of several self-trapped optical channels which survive a long distance. We have chosen this intensity because it corresponds to one of those used in the experiments [4]. We estimate the full width at half maximum (FWHM) of the arising filaments to be around 10 μm, in good agreement with the experimental measurements. Figure 1(b) shows the last stage of a simulation with $\Phi_0^2 = 0.25$, corresponding to the PW with the highest Γ_{max}. In fact, because this PW possesses the shortest longitudinal scale of destabilization, it can be seen in Fig. 1(b) that after filament formation some domains are formed due to coalescence processes between self-guiding structures. The final example, in Fig. 1(c), shows a stable PW of $\Phi_0^2 = 0.64$. This is a very interesting illustration of the phenomenon called *modulational instability suppression* (MIS). For $\Phi_0^2 > 0.5$, the linear perturbational modes decrease exponentially, thus leading to a suppression of the modulational instability which could be observed in real experiments. To our knowledge, this would constitute the first example of beam stabilization in a nonlinear optical medium obtained just by changing the input intensity.

Moreover, when the considered perturbations are intense enough, the quantity Γ_{max} acquires a greater relevancy since its inverse value yields the characteristic longitudinal scale of instability development $\Lambda_{||}$ [16]. In a first approximation, we consider the filamentation regime to be described by the coefficient $\Lambda_{||}$ as well as by the quantity $\Lambda_{\perp} = \pi/K_{\perp}^{max}$, which univocally characterizes the transverse spatial scale of the emerging filaments [9,16]. We are assuming throughout this paper that optical filaments are axially symmetric so that $\Lambda_{\perp}$ is valid for both transverse coordinates (χ, ζ). In general, both quantities ($\Lambda_{||}, \Lambda_{\perp}$) are useful in estimating the order of magnitude of different spatial instability scales, but their agreement with both simulations and experiments can be rather qualitative due to the existence of different filamentation regimes, radial perturbations, nonlinear responses, inhomogeneities in the medium, coalescence processes between filaments, and so on. In any case, as multiple filamentation appears as a consequence of modulational instability of the corresponding field, the linear stability analysis should be at least qualitatively correct at the leading order, where other nonlinear processes are not considered to be involved.

In Fig. 2, we have selected a transverse cut of the three paradigmatic PWs considered above (see Fig. 1) and we have determined their peak intensity along the propagation. As it can be appreciated, the perturbed PW with $\Phi_0^2 = 0.64$ [solid (blue) line] features a quasiconstant intensity during the whole simulation, illustrating the MIS process. However, for $\Phi_0^2 = 0.25$ [dashed (orange) line] and $\Phi_0^2 = 0.045$ (dotted line), a dramatic increase of the peak intensity with η is observed, indicating the destabilization of the initial conditions. Furthermore, there is a substantial difference in the longitudinal instability scale of both situations. It can be appreciated that $\Phi_0^2 = 0.25$ (PW featuring the highest Γ_{max}) displays a shorter instability scale than $\Phi_0^2 = 0.045$. Hereafter, we compare this numerical result with the theory as well as the predictions of the stability analysis for the experimental parameters considered by Centurion *et al.* [4], who observed the filamentation process performed via femtosecond pulses propagating in CS$_2$. Using pulses of peak intensity $I_p = 0.68$ GW/mm^2, they measured a mean filament size of 12 μm, in good agreement with our estimation. Moreover, the transverse scale of the filaments predicted by our linear stability analysis for their experimental configuration is $\Lambda_{\perp} = \pi/(\Phi_0^2 - 2\Phi_0^4)^{\frac{1}{2}}$, or $\Lambda_{\perp} \approx 16.45$ μm in dimensional units, which is also consistent with the sizes measured in Ref. [4]. This can be interpreted as further theoretical proof of the validity of the CQ model in describing the dynamics of femtosecond optical pulses propagating in CS$_2$.

On the other hand, the longitudinal scale of instability development $\Lambda_{||}$ can be estimated as $\Lambda_{||} \approx \Gamma_{max}^{-1} = 24.4$ (0.7 mm in dimensional units). This scale was not directly characterized by Centurion *et al.* in Ref. [4]. Nevertheless, they found completely developed filaments on a scale of 5 mm, which is compatible with our value of $\Lambda_{||}$ and constitutes a rough estimation of the propagation distance for the filaments when they start to grow up. Note that for $\Phi_0^2 = 0.25$ we get $\Lambda_{||} = 8$, thus justifying the shorter characteristic scale of instability development observed in Fig. 2.

While our analytical and numerical results for $\Lambda_{\perp}$ are both in good agreement with the experiment of Ref. [4], the estimations for $\Lambda_{||}$ turn out to be less accurate. This is due to the fact that in the simulations we have perturbed the homogeneous distributions with random noise instead of using harmonic perturbations with fixed $K_{\perp}$. In fact, we have checked that using harmonic perturbations leads to smaller

values for $\Lambda_\parallel$ by a factor of ~ 3, getting closer to the analytical calculation.

These results show that, in spite of its simplicity, the linear stability analysis not only provides good insight into the physics but also can be used to obtain quantitative useful predictions for the experiments of filamentation in CS_2.

IV. LIQUID LIGHT SOLITONS ARISING BY COALESCENCE

In this section we show through numerical simulations a mechanism for the dynamical excitation of so-called liquid light condensates [11] in media with CQ nonlinearity, by means of spatial control of the filamentation regime and coalescence processes between self-guided optical channels. Furthermore, we discuss the possibility of observation of these structures in the experiments with CS_2.

As a starting point, we have considered an initial condition for our simulations consisting of a broad extended laser pulse with random noise fluctuations added. Group-velocity dispersion effects are not considered here since it is justified to assume that the temporal profile of the pulse does not change during short propagation distances through CS_2 [4]. We model this light distribution with a wide flat-top profile represented by the following function:

$$\Omega = A_{bg}(0.25\{[1 + \tanh(\rho + \omega_{bg})][1 - \tanh(\rho - \omega_{bg})]\}),$$
(7)

where A_{bg} is the peak amplitude of the light pulse, $\rho = \sqrt{\chi^2 + \zeta^2}$ is the radial coordinate, and ω_{bg} is the mean radius. We have performed all simulations fixing $A_{bg} = 0.2$ and $\omega_{bg} = 1000$. As we restrict the experiment to a small region located at the center of the pulse, we can think of the domain delimited by Ω as part of a plane wave, since boundary effects (e.g., near-field diffraction) will not affect our results within the longitudinal scale imposed by the common experimental setups. We explore the case $A_{bg} = 0.2$, corresponding to a modulationally unstable plane wave [17] as we have discussed above, although the same qualitative behavior is obtained whenever $\Gamma_{max} > 0$ (see Fig. 1).

By adding an inhomogeneity to the light distribution of Eq. (7), we are able to manage the filamentation regime. In fact, we have induced a *small-scale Gaussian fluctuation* (SGF) of amplitude $A_G = 0.5071$ and width $\omega_G = 30$, located at the center of the bidimensional spatial profile Ω, in order to select a small region where filamentation will first appear. Notice the scale difference between the two counterparts. Then by overlapping both structures Ω and SGF, we generate a spatially inhomogeneous profile Φ_{in} with a peak intensity $|\Phi_{in}|^2 = 0.5$, which corresponds to that of the plane wave defining the boundary between the stable and unstable PW solutions of Eq. (1) [17].

The evolution dynamics of such a light distribution is illustrated in Fig. 3. In this figure, the panels show our small region of interest $[-75 < \chi, \zeta < 75]$. The initial condition is plotted in Fig. 3(a). Once the pulse has entered the medium, the SGF starts to self-focus. It is remarkable how such a process is quickly counteracted by the self-defocusing nonlinearity. As a result, a bright hot spot is observed at the distribu-
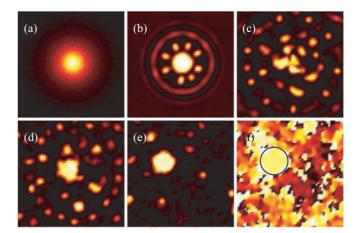

FIG. 3. (Color online) Intensity pseudocolor plots of the SGF evolution in the presence of an unstable homogeneous background. The intensity snapshots correspond to a spatial domain $[-75 < \chi, \zeta < 75]$ at several propagation distances, namely, (a) $\eta = 0$, (b) $\eta = 80$, (c) $\eta = 150$, (d) $\eta = 200$, and (e) $\eta = 1000$. Panel (f) displays the phase map of the field depicted in panel (e). From this phase structure, it can be stated that the light condensate appearing at the last stage of the propagation is a coherent light structure since the color within the region where it is located [see (blue) circle in panel (f)] is homogeneous.

tion centroid and diffractive rings representing shockwaves due to "background-fluctuation" interplay appear (see (b) snapshot).

The spectral properties of these waves (usually referred as *conical emissions*) have been studied in [18]. They give support to the formation of new filaments from pulse MI. Hereafter, we will discuss how to control the shock-wave propagation in order to stimulate the appearance of several filaments surrounding the hot spot [see Fig. 3(b)]. The key point is to generate a SGF in a precise way by using phase masks [5] and techniques like pulse shaping [19]. To excite wide liquid solitons, we propose to surround the main custom-generated light structure, which is roughly similar to a top-flat beam, with a critical number of filaments located close to it. In fact, the solitons are statistical attractors due to their high internal energy. The *satellite filaments* are then used to provide an energy source for the central seed so that its power could be increased by coalescence processes, if the phases of the soliton and the filament match. As shown in Fig. 3(c), there is indeed a dynamical energy exchange between filaments and hot spot during propagation. As a result, all solitonic structures are both created and annihilated several times [Fig. 3(c)], until a wider coherent structure with almost constant peak intensity arises [Fig. 3(d)]. As a consequence, the emerging liquid light soliton [11] is strongly perturbed by the energy excess released in the collective coalescence. Nevertheless, from Fig. 3(e) we see that after a large propagation distance the flat-topped soliton features an improved radial symmetry, and the energy excess is radiated in the form of linear modes.

In Fig. 3(f) we also show the phase map corresponding to the intensity plot displayed in Fig. 3(e). We see within the region where the condensate is placed [highlighted with a (blue) circle] that the phase structure is homogeneous.
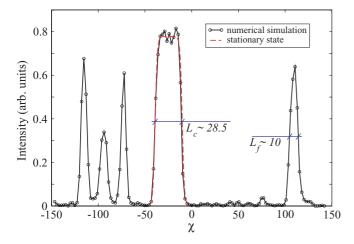
FIG. 4. (Color online) Transverse intensity profile of the filament distribution (black solid line) at $\eta = 5000$, with a superposed transverse profile of an eigenstate [dashed (red) line] of Eq. (2) with propagation constant $\gamma = 0.173$. The agreement between both contours is reasonable. FWHMs [delimited with solid (blue) lines] of the different-sized filaments represented in the figure have been estimated to be $L_c \approx 28.5$ (flat-topped soliton) and $L_f \approx 10$ (Kerr-type soliton). The spatial coordinate is $\chi \in [-150, 150]$.

Finally, we have checked the transverse size of the distribution after a huge propagation distance, $\eta = 5000$. This allows the light condensate to relax toward a stationary state, thus minimizing random profile variations due to surface modes. In Fig. 4, we have compared this extracted profile with that of a stationary solution of Eq. (2). The agreement between the transverse profiles corresponding to this simulation and the stationary mode is remarkable. This completes the demonstration that this nonlinear structure observed in our simulations is a true flat-topped CQ soliton.

To determine whether this kind of flat-top transverse mode has been observed in the experiments with CS_2 [4], we have estimated their transverse size and found that it would lie around the value $L_c \approx 28.5$ (30.2 μm in dimensional units). This is almost three times greater than the size of the optical filaments measured in Ref. [4]. We thus conclude that Centurion *et al.* have not reached the threshold to produce flat-top, liquid light solitons.

On the other hand, on the right-hand side of the light condensate displayed in Fig. 4, we also see a completely developed self-guided light channel of size $L_f \approx 10$ (10.6 μm in dimensional units), which closely resembles those observed by Centurion *et al.* This is a further demonstration that our simulations reasonably reproduce the existing observations, besides providing a guide for the new managed production of the higher-power flat-top solitons.

V. CONCLUSIONS

In this paper, we have provided theoretical support for recent experiments on filamentation of ultrashort pulses propagating through carbon disulfide by means of approximate analytical methods and numerical simulations of propagation. The agreement between our calculations and the experimental outcomes is remarkable, taking into account that we have developed the theoretical description assuming a quintic coefficient n_4 which has not been measured in the laboratory. We have shown that under certain conditions, a suppression of the modulational instability could be observed in such media over an intensity threshold. We have also described a procedure for indirect excitation of flat-top solitons in pure CQ materials, and we have argued that these nonlinear structures have not been observed experimentally. Very remarkably, recent experiments with air and other gases have revealed their CQ nature via measurement of their high-order nonlinear coefficients [14]. Thus, our results open the door to the quest for liquid light condensates in real experiments.

[1] S. Skupin *et al.*, Phys. Rev. E **70**, 046602 (2004).

[2] L. Bergé *et al.*, Phys. Rev. Lett. **92**, 225002 (2004); C. Ruiz, J. S. Roman, C. Mendez, V. Diaz, L. Plaja, I. Arias, and L. Roso, *ibid.* **95**, 053905 (2005).

[3] A. Dubietis, G. Tamosauskas, I. Diomin, and A. Varanavicius, Opt. Lett. **28**, 1269 (2003).

[4] M. Centurion, Y. Pu, M. Tsang, and D. Psaltis, Phys. Rev. A **71**, 063811 (2005); **74**, 069902(E) (2006).

[5] P. Rohwetter, M. Queisser, K. Stelmaszczyk, M. Fechner, and L. Woste, Phys. Rev. A **77**, 013812 (2008).

[6] A. H. Piekara, J. S. Moore, and M. S. Feld, Phys. Rev. A **9**, 1403 (1974).

[7] K. Dimitrievski *et al.*, Phys. Lett. A **248**, 369 (1998).

[8] Ting-Ting Xi, Xin Lu, and Jie Zhang, Phys. Rev. Lett. **96**, 025003 (2006).

[9] S. Tzortzakis, L. Berge, A. Couairon, M. Franco, B. Prade, and A. Mysyrowicz, Phys. Rev. Lett. **86**, 5470 (2001); A. Couairon, Phys. Rev. A **68**, 015801 (2003).

[10] M. Quiroga-Teixeiro and H. Michinel, J. Opt. Soc. Am. B **14**, 2004 (1997); M. L. Quiroga-Teixeiro, A. Berntson, and H. Michinel, *ibid.* **16**, 1697 (1999).

[11] H. Michinel, J. Campo-Táboas, R. García-Fernández, J. R. Salgueiro and M. L. Quiroga-Teixeiro, Phys. Rev. E **65**, 066604 (2002); H. Michinel, M. J. Paz-Alonso, and V. M. Pérez-García, Phys. Rev. Lett. **96**, 023903 (2006).

[12] D. Novoa, H. Michinel, and D. Tommasini, Phys. Rev. Lett. **103**, 023903 (2009).

[13] F. Smektala, C. Quemard, V. Couderc, and A. Barthelemy, J. Non-Cryst. Solids **274**, 232 (2000).

[14] V. Loriot *et al.*, Opt. Express **17** 13429 (2009).

[15] R. A. Ganeev *et al.*, Appl. Phys. B **78**, 433 (2004).

[16] V. I. Bespalov and V. I. Talanov, JETP Lett. **3**, 307 (1966).

[17] D. Novoa, H. Michinel, D. Tommasini, and María I. Rodas-Verde, Physica D **238**, 1490 (2009).

[18] E. T. J. Nibbering *et al.*, Opt. Lett. **21**, 62 (1996).

[19] M. R. Fetterman *et al.*, Opt. Express **3**, 366 (1998).